

Surface modification of the CoO loaded BiVO photoanodes with ultrathin *p*-type NiO layers for the improved solar water oxidation

Miao Zhong, Takashi Hisatomi, Yongbo Kuang, Jiao Zhao, Min Liu, Akihito Iwase, Qingxin Jia, Hiroshi Nishiyama, Tsutomu Minegishi, Mamiko Nakabayashi, Naoya Shibata, Ryo Niishiro, Chisato Katayama, Hidetaka Shibano, Masao Katayama, Akihiko Kudo, Taro Yamada, and Kazunari Domen

J. Am. Chem. Soc., **Just Accepted Manuscript** • Publication Date (Web): 24 Mar 2015

Downloaded from <http://pubs.acs.org> on March 24, 2015

Just Accepted

“Just Accepted” manuscripts have been peer-reviewed and accepted for publication. They are posted online prior to technical editing, formatting for publication and author proofing. The American Chemical Society provides “Just Accepted” as a free service to the research community to expedite the dissemination of scientific material as soon as possible after acceptance. “Just Accepted” manuscripts appear in full in PDF format accompanied by an HTML abstract. “Just Accepted” manuscripts have been fully peer reviewed, but should not be considered the official version of record. They are accessible to all readers and citable by the Digital Object Identifier (DOI®). “Just Accepted” is an optional service offered to authors. Therefore, the “Just Accepted” Web site may not include all articles that will be published in the journal. After a manuscript is technically edited and formatted, it will be removed from the “Just Accepted” Web site and published as an ASAP article. Note that technical editing may introduce minor changes to the manuscript text and/or graphics which could affect content, and all legal disclaimers and ethical guidelines that apply to the journal pertain. ACS cannot be held responsible for errors or consequences arising from the use of information contained in these “Just Accepted” manuscripts.



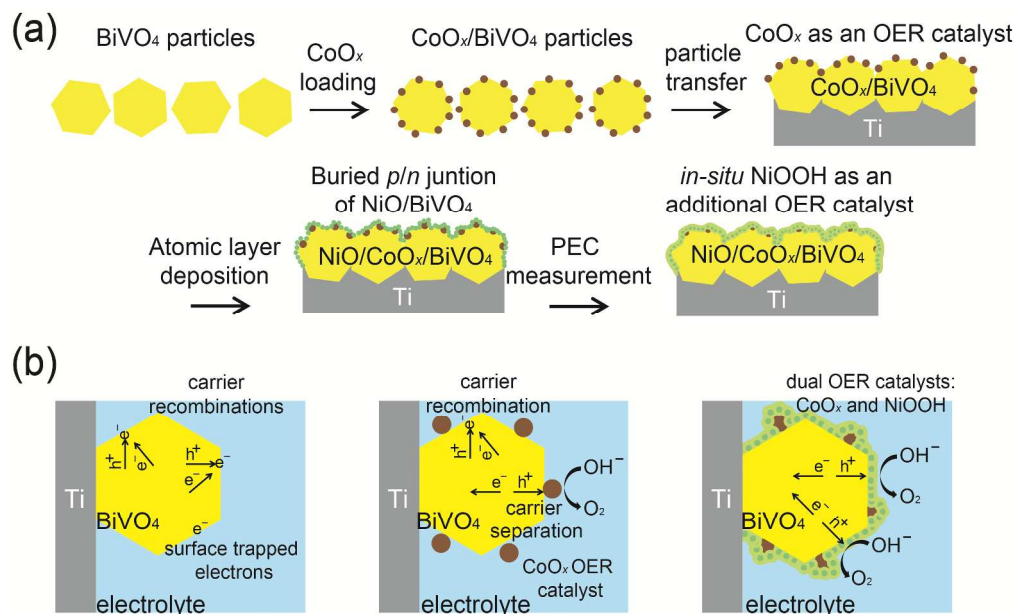


Figure 1. Fabrication of the NiOOH/NiO/CoO_x/BiVO₄/Ti photoanode and the proposed photogenerated carrier transfer process. (a) Fabrication of the NiOOH/NiO/CoO_x/BiVO₄ photoanode, including 1) synthesis of BiVO₄ particles, 2) impregnation of CoO_x on BiVO₄ with calcination, 3) sputtering of Ti metal on CoO_x/BiVO₄ particles and preparation of CoO_x/BiVO₄/Ti photoanode by the particle-transfer process, 4) Atomic layer deposition of NiO on the CoO_x/BiVO₄/Ti photoanode, and, 5) *in-situ* formation of the NiOOH/NiO/CoO_x/BiVO₄/Ti structure during PEC measurement. (b) Proposed recombination/separation processes of the photogenerated carriers in the bare BiVO₄/Ti, the CoO_x/BiVO₄/Ti, and the NiOOH/NiO/CoO_x/BiVO₄/Ti photoanodes. The conformal deposition of NiO with the *in-situ* formed NiOOH on the CoO_x/BiVO₄ surface effectively passivates the surface states, reduces the carrier recombination, and therefore enhances the PEC performances.

1064x651mm (72 x 72 DPI)

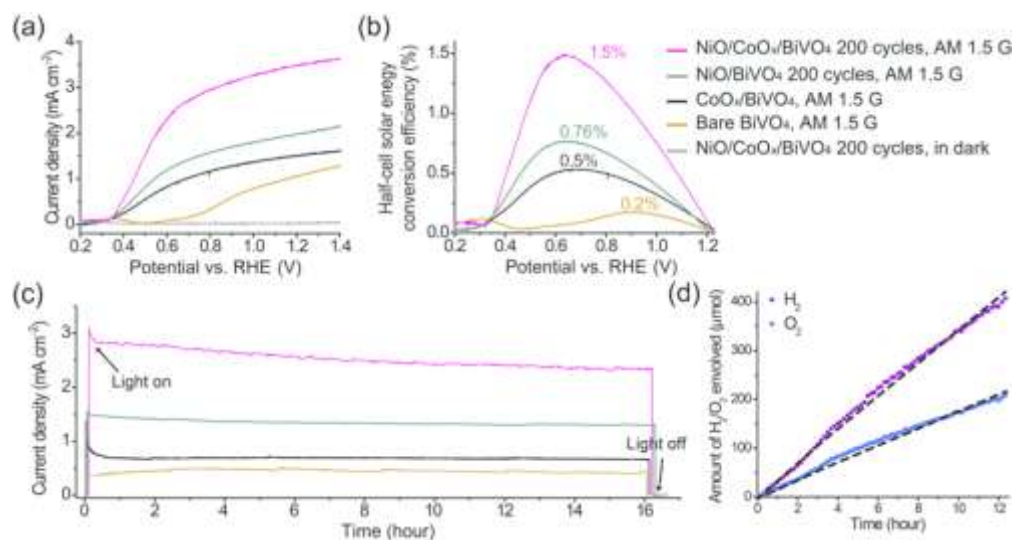


Figure 2. Solar-driven PEC performances of the BiVO₄ photoanodes in water oxidation. The PEC performances of the bare BiVO₄, the CoO_x/BiVO₄ (CoO_x 1wt%) and the NiO/CoO_x/BiVO₄ (ALD 200 cycles, CoO_x 1wt%) photoanodes in 0.1 M KPi solution at pH 7: (a) LSV scans in dark and under AM 1.5G illumination, scan rate: 10 mV s⁻¹, (b) half-cell solar conversion efficiencies, (c) j-t curves at 0.8 VRHE, j is recorded at a time interval of 1 min, (d) the H₂ and O₂ evolution at 1.0 VRHE, the dashed curves indicate the H₂ and O₂ evolution with 100% Faraday efficiency.

282x149mm (72 x 72 DPI)

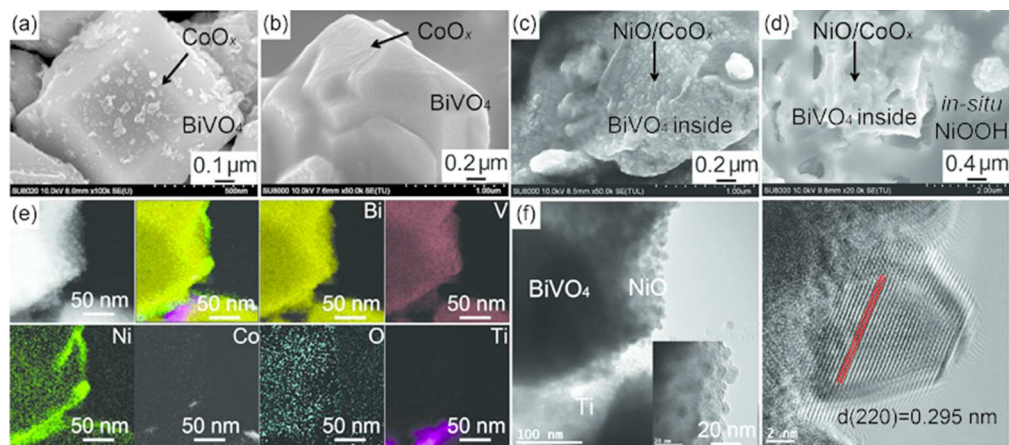


Figure 3. SEM, STEM and EDS characterizations. (a-d), The morphologies of the CoOx/BiVO₄ (CoOx 1wt%) photoanode before (a) and after (b) the 30-minute PEC measurements in 0.1 M KPi solution at pH 7, and, the NiO/CoOx/BiVO₄ (~ 6 nm NiO by 200-cycle ALD, CoOx 1wt%) photoanode before (c) and after the 30-minute PEC measurements in 0.1 M KPi solution at pH 7 (d). (e) EDS mapping images of the NiO/CoOx/BiVO₄ particle in STEM. (f) HRTEM images of the NiO/CoOx/BiVO₄ particle. 282x124mm (72 x 72 DPI)

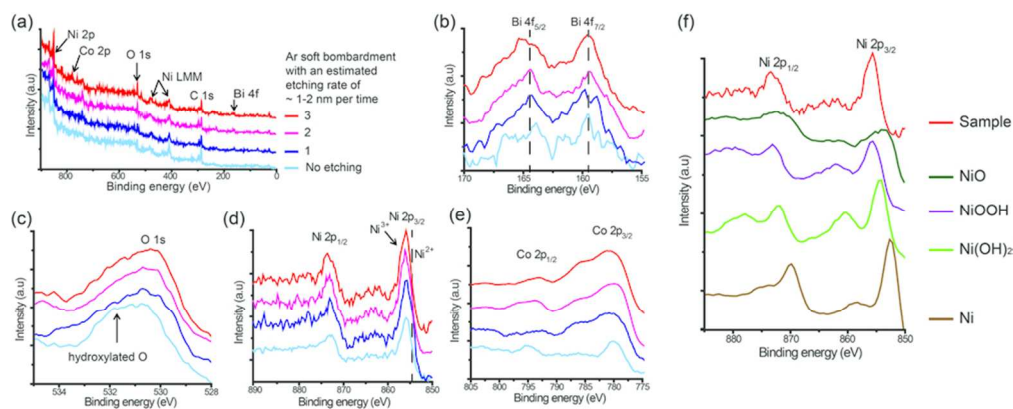


Figure 4. XPS analyses. (a-e), XPS analyses of the NiO/CoOx/BiVO₄ photoanode after the PEC measurements under soft Ar bombardment: (a) XPS survey spectra, (b) high resolution XPS spectra of Bi 4f, (c) O 1s, (d) Ni 2p and (e) Co 2p. (f) High resolution XPS Ni 2p spectra obtained with the Ni metal, the NiO, the Ni(OH)₂, the NiOOH and the NiO/CoOx/BiVO₄ after-PEC-measurement photoanode. 352x140mm (72 x 72 DPI)

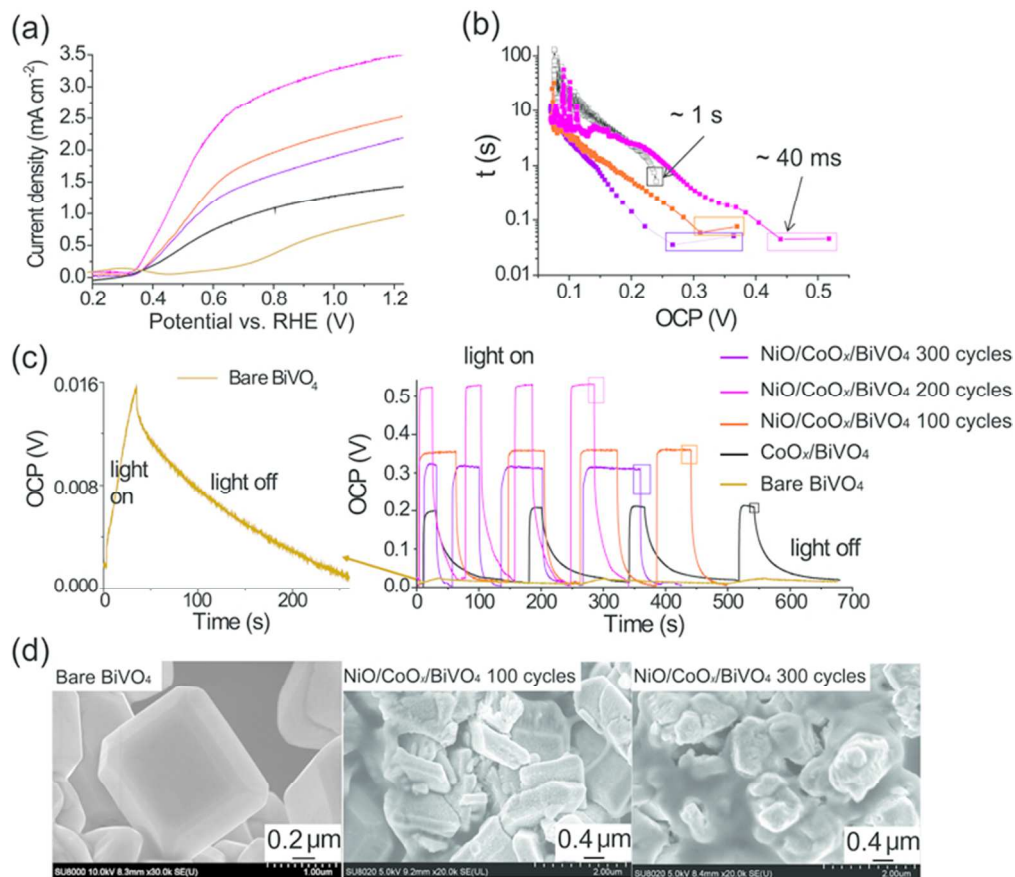


Figure 5. ALD NiO thickness dependent study. (a) The LSV scans under AM 1.5G illumination of the bare BiVO₄, the CoO_x/BiVO₄ (CoO_x 1wt%) and NiO/CoO_x/BiVO₄ (ALD 100, 200 and 300 cycles, CoO_x 1wt%) photoanodes in 0.1 M KPi solution at pH 7. (b) The carrier lifetime derived from OCP-decay curve at the transient when illumination is removed at the OC condition and plotted as a function of OCP in a log-rhythm scale. The results were measured in 0.1 M KPi solution at pH 7. (c) The OCP values in 0.1 M KPi solution at pH 7 under AM 1.5G illumination and in dark. (d) SEM images of the bare/BiVO₄, the 100-cycle NiO/CoO_x/BiVO₄ and 300-cycle NiO/CoO_x/BiVO₄ photoanodes after the PEC measurement.

Surface modification of the CoO_x loaded BiVO_4 photoanodes with ultrathin p -type NiO layers for the improved solar water oxidation

Miao Zhong^{† ‡}, Takashi Hisatomi^{† ‡}, Yongbo Kuang^{† ‡}, Jiao Zhao^{† ‡}, Min Liu^{† ‡}, Akihide Iwase[§], Qingxin Jia^{‡ §}, Hiroshi Nishiyama^{† ‡}, Tsutomu Minegishi^{† ‡}, Mamiko Nakabayashi[¶], Naoya Shibata[¶], Ryo Niishiro^{‡ #}, Chisato Katayama^{‡ ⊥}, Hidetaka Shibano[‡], Masao Katayama^{† ‡}, Akihiko Kudo^{‡ §}, Taro Yamada^{† ‡} and Kazunari Domen^{* † ‡}

[†] Department of Chemical System Engineering, The University of Tokyo, 7-3-1 Hongo, Bunkyo-ku, Tokyo 113-8656, Japan

[‡] Japan Technological Research Association of Artificial Photosynthetic Chemical Process (ARPCChem), 5-1-5 Kashiwanoha, Kashiwa-shi, 277-8589 Chiba, Japan

[§] Department of Applied Chemistry, Tokyo University of Science, 1-3 Kagurazaka, Shinjuku-ku, Tokyo 162-8601, Japan

[¶] Institute of Engineering Innovation, The University of Tokyo, 2-11-16, Yayoi, Bunkyo-ku, Tokyo 113-8656, Japan.

[#] Mitsui Chemicals, Inc., 580-32 Nagaura, Sodegaura, 299-0265 Chiba, Japan

[⊥] Fujifilm Corporation, 577, Ushijima, Kaisei-Machi, Ashigarakami-gun, 258-8577 Kanagawa, Japan

ABSTRACT: Photoelectrochemical (PEC) devices that use semiconductors to absorb solar light for water splitting offer a promising way toward the future scalable production of renewable hydrogen fuels. However, the charge recombination in the photoanode/electrolyte (solid/liquid) junction is a major energy loss and hampers the PEC performance from being efficient. Here, we show that this problem is addressed by the conformal deposition of an ultrathin p -type NiO layer on the photoanode to create a buried p/n junction as well as to reduce the charge recombination at the surface trapping states for the enlarged surface band bending. Further, the *in-situ* formed hydroxyl-rich and hydroxyl-ion-permeable NiOOH enables the dual catalysts of CoO_x and NiOOH for the improved water oxidation activity. Compared to the CoO_x loaded BiVO_4 ($\text{CoO}_x/\text{BiVO}_4$) photoanode, the ~ 6 nm NiO deposited $\text{NiO}/\text{CoO}_x/\text{BiVO}_4$ photoanode triples the photocurrent density at 0.6 V_{RHE} under AM 1.5G illumination and enables a 1.5% half-cell solar-to-hydrogen efficiency. Stoichiometric oxygen and hydrogen are generated with Faraday efficiency of unity over 12 h. This strategy could be applied to other narrow-band-gap semiconducting photoanodes toward the low-cost solar fuel generation devices.

Introduction

In response to the rising global energy demand and the corresponding environmental concerns, producing clean and renewable fuels becomes increasingly essential¹⁻⁶. Among a range of possible fuel candidates, hydrogen is one of the most promises because it is carbon-neutral, high in energy density and easily portable. It releases energy after combustion with oxygen and leaves the only by-product of water. In this regard, extracting hydrogen from water by PEC devices using solar light is of particular interest, which enables recyclable use of hydrogen fuel in a green and sustainable way⁷⁻¹³.

Constructing a high-performance PEC device generally requires highly photoactive and durable photocathodes and photoanodes for the water reduction and water oxidation reactions. Benefiting from the extensive experience gained in the electronic and solar cell industry, significant improvements have been achieved in development of the photocathodes¹⁴⁻¹⁸. The important p -type solar cell semiconductors such as silicon, III-V and I-III-VI₂ compounds are excellent light absorbers with high carrier mobility and therefore enable high solar-to-hydrogen conversion efficiencies when used as photocathodes in PEC cells. However, limited success has been achieved in photoanodes.

To expedite the PEC water splitting toward practical applications, the development of efficient and stable photoanode is crucial. The photoanodes are operated in a highly oxidizing environment, and thus the above-mentioned high-performance solar cell materials, which are extremely prone to photo-corrosion, are difficult for direct use in photoanodes.

Metal oxides are superior candidates for photoanodes because they are relatively stable for water oxidation reactions¹⁹⁻²¹. However, the poor charge separation in the metal oxides is a major limitation, preventing their PEC performances from being optimal. To enhance the charge separation, previous researches mainly focused on 1) synthesizing high-quality nanostructures with the sizes smaller than the hole diffusion length²²⁻²⁴ and 2) increasing the electrical conductivity by donor-type dopants to reduce the resistive loss in the bulk with the applied electrical bias^{25,26}. Although these approaches have significantly improved the PEC performances, further efforts are still needed to enhance the mechanical strength of nanostructures, to realize a controllable doping profile and to reduce the external energy input of the applied bias.

In addition to the above mentioned approaches which mainly aim to suppress the charge recombination in the bulk, another significant energy loss attributed to the charge recombination at the photoanode surface trapped states is not fully addressed. A simple and potentially efficient way to deal with this issue is to create a buried *p/n* junction at the photoanode surface. In this way, the photogenerated holes are thermodynamically extracted from the photoanode bulk and stored in the surface *p*-type material with a prolonged lifetime. The conformal deposition of an ultrathin *p*-type layer can also effectively passivate the surface trapped electrons for the reduced surface charge recombination. In addition, the deposited ultrathin *p*-type layer enables the efficient migration of the holes to the electrolyte with a small resistive loss within this layer. Among various *p*-type materials, NiO is particularly promising because it has an appropriate valence band position^{27,28} for the oxygen evolution reactions (OERs) and a strong resistance to photo-corrosion in neutral and alkaline electrolytes.

Besides the efficient charge separation, a fast OER kinetics is of equal importance for high PEC performances. This requires the development of effective OER catalysts to lower the over-potential needed for the four-electron involved OERs. Solid-state catalysts such as IrO_x ²⁹, CoO_x ^{30,31}, NiO ^{32,33} and NiFe_2O_4 ³⁴ have long been regarded as the promising electro-catalysts for dark OERs, however, only moderate activities have been achieved so far in the PEC OERs under light illumination. The amorphous “Co-Pi” discovered by Kanan and Nocera exhibits an excellent dark OER activity and durability^{35,36}. Also, the simple and low-cost fabrication process makes it amenable for mass production. However, the ultrathin “Co-Pi” layer dissolves in the pure phosphate solution at neutral pH conditions,

which hinders the use of ultrathin “Co-Pi” layer for efficient PEC OERs with a minimized potential loss at this “Co-Pi” layer. To solve this problem, surface deposition of another ultrathin, non-dissolving and hydroxyl-ion permeable OER catalyst layer over the “CoPi” or CoO_x is a feasible approach.

In this study, we demonstrate the efficient and stable particle-transferred photoanode made of cobalt oxide loaded BiVO_4 ($\text{CoO}_x/\text{BiVO}_4$) particles with Ti metal sputtered on the backside to improve electrical conductivity and an ultrathin and conformal *p*-type NiO layer deposited on the surfaces to create a buried surface *p/n* junction for the enhanced charge separation. The *in-situ* formed hydroxyl-ion permeable NiOOH on the photoanode surface during the PEC measurements further enables the dual OER catalysts of CoO_x and NiOOH for the improved PEC performances (Figure 1).

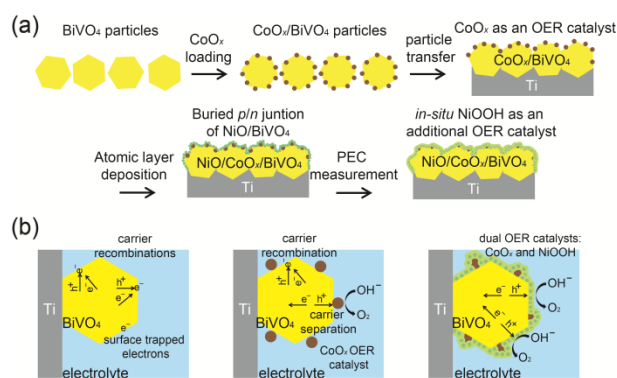


Figure 1. Fabrication of the NiOOH/NiO/CoO_x/BiVO₄/Ti photoanode and the proposed photogenerated carrier transfer process. (a) Fabrication of the NiOOH/NiO/CoO_x/BiVO₄ photoanode, including 1) synthesis of BiVO₄ particles, 2) impregnation of CoO_x on BiVO₄ with calcination, 3) sputtering of Ti metal on CoO_x/BiVO₄ particles and preparation of CoO_x/BiVO₄/Ti photoanode by the particle-transfer process, 4) Atomic layer deposition of NiO on the CoO_x/BiVO₄/Ti photoanode, and, 5) *in-situ* formation of the NiOOH/NiO/CoO_x/BiVO₄/Ti structure during PEC measurement. (b) Proposed recombination/separation processes of the photogenerated carriers in the bare BiVO₄/Ti, the CoO_x/BiVO₄/Ti, and the NiOOH/NiO/CoO_x/BiVO₄/Ti photoanodes. The conformal deposition of NiO with the *in-situ* formed NiOOH on the CoO_x/BiVO₄ surface effectively passivates the surface states, reduces the carrier recombination, and therefore enhances the PEC performances.

Experimental Section

Sample fabrication. The NiO/CoO_x/BiVO₄ photoanode was fabricated by the following procedures: 1) synthesizing crystalline BiVO₄ particles, 2) loading CoO_x catalysts on the BiVO₄ particles, 3) drop-casting the CoO_x/BiVO₄ particles on glass substrates, sputtering Ti metals on the CoO_x/BiVO₄ particles and transferring the Ti-sputtered CoO_x/BiVO₄ particles as electrodes onto other glass substrates (the particle-transfer method)³⁷, and 4) depositing NiO on the surfaces of CoO_x/BiVO₄ elec-

trodes by the ALD using Beneq TFS 200. The experimental details of each procedure are provided in the Supporting information (Figure S1). The photoanode with a uniform NiO/CoO_x/BiVO₄ surface coverage can always be obtained by our controlled fabrication method. Generally, over 80% of the PEC performance is ensured.

Measurements. The SEM observations were carried out using a Hitachi SU8020 system. The STEM and EDS analyses were conducted with ARM-200F microscopes and a JED-2300T EDS system. The XPS analyses were performed using Mg K α (1253.6 eV) photon energy. During the X-ray photoelectron spectroscopy (XPS) depth profile studies, slow Ar ion etching with an estimated etching thickness of 1-2 nm/time was used for the depth profile study. Binding energy peak shifts due to any charging were normalized with the C 1s peak set to 284.8 eV.

The PEC performances were investigated using a three-electrode electrochemical configuration in a 0.1 M KPi buffer solution at pH = 7 under simulated sunlight illumination (SAN-EI electronic, XES40S1, AM 1.5G, 100 mW cm⁻²). The electrolyte was stirred and bubbled with Ar gas before the measurements. An Ag/AgCl electrode in saturated KCl solution was used as a reference electrode and a Pt coil was used as a counter electrode. The measured potentials versus Ag/AgCl were all converted to the reversible hydrogen electrode scale according to the Nernst equation,

$$V_{RHE} = V_{Ag/AgCl} + 0.059 pH + V_{Ag/AgCl}^{\circ}$$

$$V_{Ag/AgCl}^{\circ} = 0.199 \text{ V at } 25^{\circ}\text{C}.$$

The potential of the working electrode was controlled by a potentiostat (Hokuto Denko, HSV-100). The scan rate is fixed at 10 mV s⁻¹ for all the PEC LSV analyses. The forward scans swept the bias from negative to positive. The solar conversion efficiency (η) is calculated from the current-potentiometry data using the following equation:

where V_{RHE} is the potential of the working electrode versus the reversible hydrogen electrode in the unit of volt,

$$\eta = \frac{(j_{light} - j_{dark})(\text{mA}\times\text{cm}^{-2}) \times (1.23 - V_{RHE})(\text{V})}{P_{sunlight}(\text{mW}\times\text{cm}^{-2})} \times 100\%$$

j_{light} and j_{dark} are the measured photocurrent density in dark and under AM 1.5G illumination, respectively, and $P_{sunlight}$ is the incident AM 1.5G irradiance.

An air-tight three-electrode PEC cell with an Ag/AgCl reference electrode and a Pt wire counter electrode was used for gas chromatography. The PEC cell was connected to a vacuum pump and a gas chromatograph. Before the measurement, the PEC cell was pumped to low vacuum and then purged with Ar flow sufficiently until no nitrogen and oxygen gases can be detected in GC. The amount of oxygen and hydrogen evolved on the photoelectrode and the Pt counter electrode were measured with a gas chromatograph (Shimadzu, GC-8A).

Results and discussion

PEC performances. The PEC performances of the bare BiVO₄, the CoO_x/BiVO₄ (CoO_x 1wt%), the NiO/BiVO₄ (~ 6 nm NiO with ALD 200 cycles) and the NiO/CoO_x/BiVO₄ (~ 6 nm NiO with ALD 200 cycles, CoO_x 1wt%) photoanodes in 0.1 M pH 7 potassium phosphate (KPi) solution are presented in Figure 2. All of the photoanodes showed low dark currents in the linear sweep voltammetry (LSV) scans, indicating that no chemical reaction occurred in dark. BiVO₄ absorbs the visible light in the solar spectrum up to 520 nm (E_g of 2.4 eV)²⁴, however, the particle-transferred bare BiVO₄ photoanode shows a low photocurrent density (j) under the simulated air mass (AM) 1.5G illumination (Figure 2a), indicating that most of the photogenerated holes are recombined before they oxidize water.

Surface loading of CoO_x (1 wt%) on the BiVO₄ can promote the charge separation³⁶ and enhance the OER activity, leading to the improved onset potential for water oxidation and also the increased PEC performance (Figure 2a). However, the obtained photocurrent density with the CoO_x/BiVO₄ photoanode is still far below the theoretical photocurrent density of the BiVO₄ calculated by converting the absorbed photons in the solar spectra. This is because the CoO_x is dispersively loaded on the BiVO₄ and it cannot fully suppress the charge recombination at the CoO_x uncovered surface areas. In addition, the CoO_x potentially dissolves in the KPi solution at neutral pH conditions, which prevents the effective use of the CoO_x surface modification for durable PEC water oxidation in moderate pH KPi electrolytes.

To cope with this issue, a *p*-type NiO layer (~ 6 nm) was conformally deposited on the CoO_x/BiVO₄ photoanodes by atomic layer deposition (ALD) to passivate the surface states as well as to create a buried *p/n* junction for the improved charge separation. The details of the NiO ALD recipes and the electrochemical characterizations are shown in the supporting information (Figure S2). Generally, the ALD NiO growth rate is estimated to be ~ 0.3 Å per cycle and the 200-cycle ALD realizes the conformal deposition of ~ 6 nm NiO (Figure S2). A unique advantage of the ALD is the conformal deposition of NiO layers with controllable thickness in the angstrom/nanometer level to wrap the BiVO₄ particles in a 3D profile (Figure S3). Importantly, the *p*-type semiconducting character of the ALD NiO is evidenced by the Mott-Schottky analysis (Figure S4) and therefore, a surface *p/n* junction effect can be anticipated.

The photocurrent density of the NiO/CoO_x/BiVO₄ photoanode reached 3.5 mA cm⁻² at 1.23 V_{RHE}, which was increased twice compared to that of the CoO_x/BiVO₄ photoanode (Figure 2a). The appearance of the anodic photocurrent at ~ 0.35 V_{RHE} from the reverse LSV scan sweeping from positive bias to negative bias indicates the onset potential of the NiO/CoO_x/BiVO₄ photoanode, ~ 50 mV cathodically shifted relative to that of the CoO_x/BiVO₄

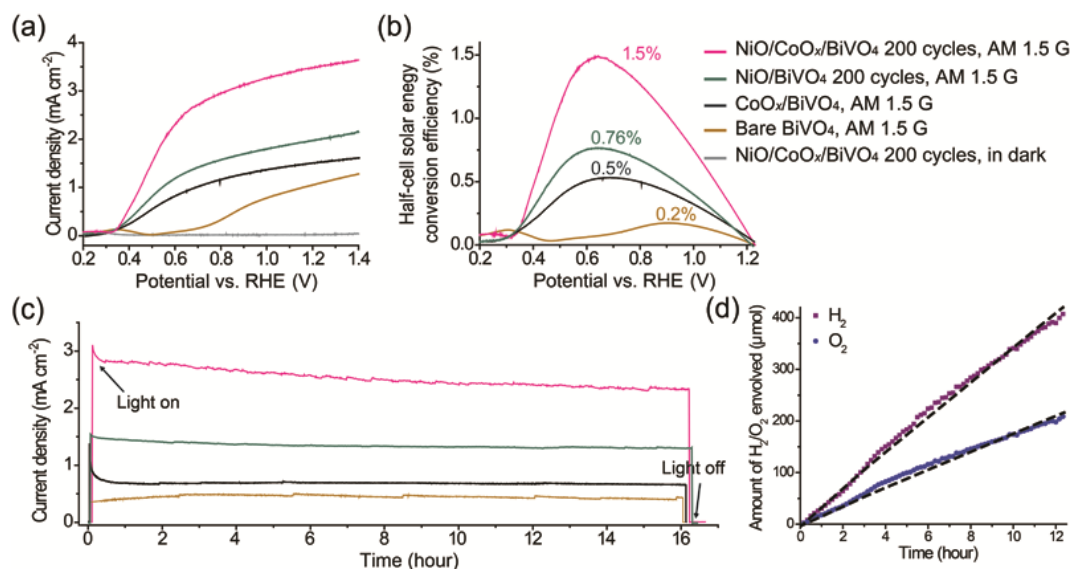


Figure 2. Solar-driven PEC performances of the BiVO_4 photoanodes in water oxidation. The PEC performances of the bare BiVO_4 , the $\text{CoO}_x/\text{BiVO}_4$ (CoO_x 1wt%) and the $\text{NiO}/\text{CoO}_x/\text{BiVO}_4$ (ALD 200 cycles, CoO_x 1wt%) photoanodes in 0.1 M KPi solution at pH 7: (a) LSV scans in dark and under AM 1.5G illumination, scan rate: 10 mV s^{-1} , (b) half-cell solar conversion efficiencies, (c) j - t curves at $0.8 V_{\text{RHE}}$, j is recorded at a time interval of 1 min, (d) the H_2 and O_2 evolution at $1.0 V_{\text{RHE}}$, the dashed curves indicate the H_2 and O_2 evolution with 100% Faraday efficiency.

photoanode (Figure S5). A rapid increase of the photocurrent density from the onset potential, representing an improved fill factor, was obtained with the $\text{NiO}/\text{CoO}_x/\text{BiVO}_4$ photoanode. The photocurrent density reached 2.5 mA cm^{-2} at $0.6 V_{\text{RHE}}$, a threefold improvement compared to the $\text{CoO}_x/\text{BiVO}_4$ photoanode. The high photocurrent density at the low potential represents a highly photoactive surface for efficient transport of holes through the photoanode surface for OERs. The half-cell solar-to-hydrogen conversion efficiency calculated from the LSV results in Figure 2a reaches 1.5% (Figure 2b), which is comparatively high among the reported single-photon photoanodes^{24,25}. The wavelength dependence of the incident photon-to-current conversion efficiency (IPCE) was examined (Figure S6). Integrating the IPCE curves using the AM 1.5G spectrum, the obtained photocurrent density agrees well with the values in the LSV curves in Figure 2a. Thus, the measured LSV data represent the steady-state PEC performance under AM 1.5G illumination.

The PEC stability of the bare BiVO_4 , the $\text{CoO}_x/\text{BiVO}_4$, the NiO/BiVO_4 and the $\text{NiO}/\text{CoO}_x/\text{BiVO}_4$ photoanodes were compared in 0.1 M KPi at pH 7 by the chronoamperometric j - t study (Figure 2c). The $\text{NiO}/\text{CoO}_x/\text{BiVO}_4$ photoanode shows a stable photocurrent density at $0.8 V_{\text{RHE}}$ under continuous AM 1.5G illumination over 16 hours with clear light on/off behaviors. Bubbles are continuously generated on the $\text{NiO}/\text{CoO}_x/\text{BiVO}_4$ surface during the stability test.

To confirm the hydrogen evolution reactions (HERs) at the Pt electrode and OERs at the $\text{NiO}/\text{CoO}_x/\text{BiVO}_4$ photoanode, the evolved gases were examined by gas chromatography (GC). The $\text{NiO}/\text{CoO}_x/\text{BiVO}_4$ photoanode was held at a constant bias of $1 V_{\text{RHE}}$ in a three-electrode con-

figuration. The evolved H_2 and O_2 gases were quantified every 10 minutes by automatic GC integration. The total amounts of the evolved H_2 and O_2 gases were 390 and 198 μmol after 12 hours (Figure 2d). No nitrogen gas was detected during the 12 hours test, indicating that there is no air leaking in our GC system. Stoichiometric evolution of H_2 and O_2 with a ratio of virtually two was obtained. The faraday efficiency for the HERs and OERs are found by counting the electrons passing through the PEC cell to be both close to 100%. These results confirm that the photocurrent was attributed to the OERs and HERs, and thus the half-cell solar-to-hydrogen conversion efficiency can be calculated using the measured LSV curves under AM 1.5G.

Characterizations. The scanning electron microscopy (SEM) images of the $\text{CoO}_x/\text{BiVO}_4$ (CoO_x 1wt%) and the $\text{NiO}/\text{CoO}_x/\text{BiVO}_4$ ($\sim 6 \text{ nm NiO}$ by 200 ALD cycles, CoO_x 1wt%) photoanodes before and after the PEC measurements are presented in Figure 3 and Figure S7. The CoO_x particles ($\sim 10\text{-}30 \text{ nm}$) were dispersively loaded on the surfaces in the as-synthesized $\text{CoO}_x/\text{BiVO}_4$ photoanode (Figure 3a). After the 30-minute PEC measurement in 0.1 M KPi solution at pH 7, small nano-granules were observed (Figure 3b). These nano-granules were likely the CoO_x *in-situ* formed during the PEC measurement³⁶. The CoO_x gradually dissolves in the KPi solution, as indicated by the decrease of the photoanodic current in LSV scans in new KPi solutions (Figure S8).

To prevent the CoO_x leaking from the surface, $\sim 6 \text{ nm NiO}$ was deposited over the $\text{CoO}_x/\text{BiVO}_4$ particles by 200-cycle ALD. As shown in Figure 3c, the NiO nano-particles were uniformly deposited on the $\text{CoO}_x/\text{BiVO}_4$ photoanode. After the 30-minute PEC measurement, thin flat and translucent films were observed on the top of NiO

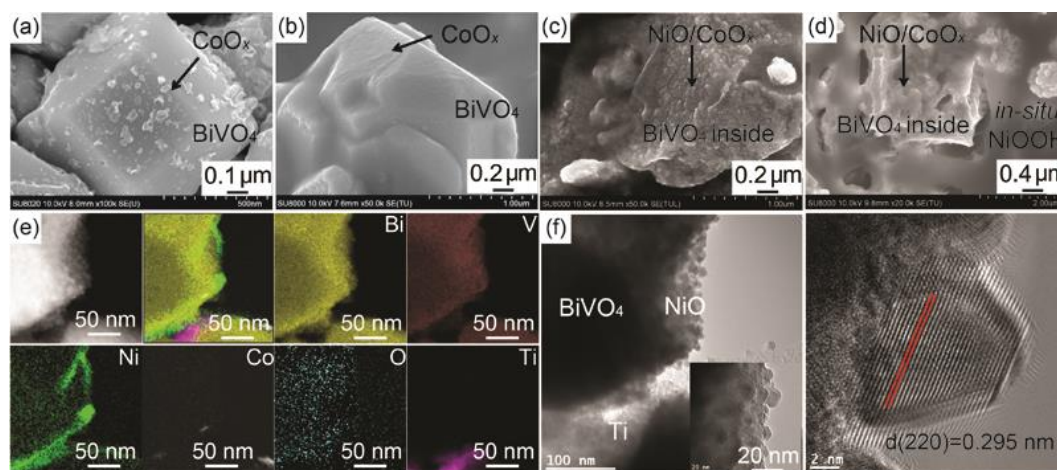


Figure 3. SEM, STEM and EDS characterizations. (a-d), The morphologies of the $\text{CoO}_x/\text{BiVO}_4$ (CoO_x 1wt%) photoanode before (a) and after (b) the 30-minute PEC measurements in 0.1 M KPi solution at pH 7, and, the $\text{NiO}/\text{CoO}_x/\text{BiVO}_4$ (~ 6 nm NiO by 200-cycle ALD, CoO_x 1wt%) photoanode before (c) and after the 30-minute PEC measurements in 0.1 M KPi solution at pH 7 (d). (e) EDS mapping images of the $\text{NiO}/\text{CoO}_x/\text{BiVO}_4$ particle in STEM. (f) HRTEM images of the $\text{NiO}/\text{CoO}_x/\text{BiVO}_4$ particle.

particles (Figure 3d). The translucent film was likely the NiOOH *in-situ* formed during the PEC measurement^{32,33}. This is evidenced by the XPS analyses as discussed later.

To characterize the structure and the crystalline quality of the $\text{NiO}/\text{CoO}_x/\text{BiVO}_4$ particles, transmission electron microscopy (TEM) and energy dispersive X-ray spectroscopy (EDS) analyses were performed. The EDS element mapping profiles in Figure 3e reveal that NiO was homogeneously deposited on the BiVO_4 surface. TEM images of the $\text{NiO}/\text{CoO}_x/\text{BiVO}_4$ particles in different magnifications are shown in Figure 3f. The size of the NiO nano-particles is in the range of 5–10 nm, which agrees well with the SEM results. The single crystal NiO nano-particle with an interplanar spacing of ~ 0.295 nm corresponding to the NiO (220) plane is clearly observed.

To ascertain the constituent compositions and the chemical states of the $\text{NiO}/\text{CoO}_x/\text{BiVO}_4$ (200-cycle ALD, CoO_x 1 wt%) photoanode after the PEC measurement (the same sample of Figure 3d), X-ray photoelectron spectroscopy (XPS) analyses were conducted. As shown in the XPS survey spectra in Figure 4a, Bi, O, Ni and Co elements were continuously detected during the soft Ar bombardment. The binding energy peak of ~ 159 eV is determined for the Bi $4f_{7/2}$, which is in coincident with the reported value²⁰. The Bi $4f_{7/2}$ and the Bi $4f_{5/2}$ peak positions remain unchanged upon Ar etching but intensities increase with Ar etching (Figure 4b), indicating more BiVO_4 is exposed with soft Ar bombardment.

Importantly, the hydroxyl O 1s peaks was observed in Figure 4c, indicating the hydroxylated surface of the $\text{NiO}/\text{CoO}_x/\text{BiVO}_4$ photoanode. It is consistent with the SEM observation of the translucent NiOOH film on the $\text{NiO}/\text{CoO}_x/\text{BiVO}_4$ surface (Figure 4d). The peak intensity ratio between the hydroxyl O 1s and the oxide state O 1s decreases with Ar etching, indicating the surface OH ions are bombarded out during the Ar bombardment. As re-

ported, the NiOOH is an OER catalyst for dark electrolysis^{24,32}. A smaller overpotential was needed to obtain the same current density with the $\text{NiO}/\text{CoO}_x/\text{FTO}$ electrode compared to the CoO_x/FTO electrode (Figure S9).

As shown in Figure 4d, the Ni $2p_{3/2}$ peaks with a predominant intensity close to a higher binding energy over 856 eV, which is more positive than the typical divalent Ni species binding energy in NiO (854–855 eV), are constantly observed in the narrow scans after Ar bombardment. This is indicative of the presence of trivalent Ni species. To further ascertain the formation of Ni^{3+} (in NiOOH) on the BiVO_4 surface, the Ni $2p_{3/2}$ XPS spectra of the $\text{NiO}/\text{CoO}_x/\text{BiVO}_4$ after the PEC measurement, the Ni metal, the NiO powder (Wako), the $\text{Ni}(\text{OH})_2$ powder (Aldrich) and the synthesized NiOOH were measured (Figure 4f). The details of the NiOOH synthesis are described in the supporting information with XRD characterizations (Figure S10). It is therefore evidenced that NiOOH was formed on the $\text{NiO}/\text{CoO}_x/\text{BiVO}_4$ photoanode surface during our PEC measurement.

The existence of the buried CoO_x in the $\text{NiO}/\text{CoO}_x/\text{BiVO}_4$ photoanode after PEC measurement is further evidenced. Co $2p_{1/2}$ and $2p_{3/2}$ peaks close to the Co^{2+} 2p binding energy positions were clearly detected in the XPS analyses (Figure 4e). Compared to the Ni signal intensity, the detected Co signal intensity is much smaller indicating that the amount of CoO_x loaded by impregnation method is much smaller compared to that of NiO by ALD. It agrees with the EDS analyses in Figure 3e. Therefore, the structure of $\text{NiOOH}/\text{NiO}/\text{CoO}_x/\text{BiVO}_4$ is inferred as shown in Figure 1.

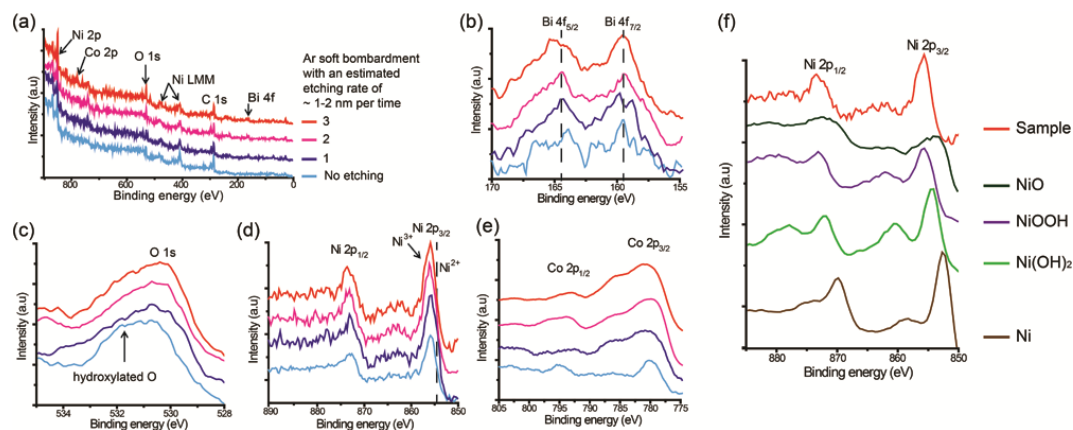


Figure 4. XPS analyses. (a-e), XPS analyses of the NiO/CoO_x/BiVO₄ photoanode after the PEC measurements under soft Ar bombardment: (a) XPS survey spectra, (b) high resolution XPS spectra of Bi 4f, (c) O 1s, (d) Ni 2p and (e) Co 2p. (f) High resolution XPS Ni 2p spectra obtained with the Ni metal, the NiO, the Ni(OH)₂, the NiOOH and the NiO/CoO_x/BiVO₄ after-PEC-measurement photoanode.

Open-circuit photovoltage and surface band bending diagrams. A *p/n* junction serves an important role in the semiconductor based electronic devices. For example, high-quality *p/n* junctions are key building blocks in solar cell devices enabling efficient charge separation to achieve high energy conversion efficiencies. In the photoanode-based half-cell water splitting scheme, the efficient charge separation is also of first importance to realize high PEC performances. Further, the separated holes on the half-cell photoanode surfaces should have a long lifetime to oxidize water before they are recombined with electrons at the surface states. Thus, the enhanced OERs is always obtained when coupled with effective OER catalysts.

To study the possible *p/n* junction effect, the PEC performances of the four BiVO₄ photoanodes in Figure 2a were measured in 0.1 M KPi solution with the presence of 1 M Na₂SO₃ as a hole scavenger under AM 1.5G illumination (Figure S11). The oxidation of sulfite is thermodynamically and kinetically easier than the oxidation of water²⁴, and therefore, it allows us to compare the charge separation abilities in different photoanodes by comparing their photocurrent density regardless the slow OER kinetics. It is observed that the photocurrent density increases from the bare BiVO₄ to the NiO/CoO_x/BiVO₄ photoanodes in the sulfite solution indicating the increased charge separation with the buried *p/n* junctions. Different from the photoelectrochemical deposition or electrochemical deposition of amorphous FeOOH²⁴, NiOOH²⁴ and CoPi^{25,35}, our impregnated CoO_x and ALD NiO are both calcined at 300 °C for more than one hour. This process helps the crystallization of CoO_x and NiO on BiVO₄ to realize the buried *p/n* junctions.

To examine the functionality of the ALD NiO layers on the CoO_x/BiVO₄ photoanodes, thickness dependence study was performed using 100- to 300-cycle ALD NiO and fixing CoO_x in 1 wt%. Compared to the CoO_x/BiVO₄

photoanode, the PEC performances of the NiO/CoO_x/BiVO₄ photoanodes (ALD 100-300 cycles) are improved (Figure 5a). It suggests that the conformal deposition of NiO on BiVO₄ surfaces forms buried *p/n* junctions and effectively passivates the BiVO₄ surface states for the enlarged charge separation. In addition, the *in-situ* formed NiOOH may further work as an OER catalyst to promote the OERs. Note that the NiOOH layer should be thin enough to efficiently transport holes through the NiOOH film for OERs. Otherwise, the electron-hole recombination occurs in the thick NiOOH film and decreases the PEC performance³²⁻³³. In our case, the NiOOH film in the 300-ALD-cycle NiO/CoO_x/BiVO₄ photoanode was apparently thicker (Figure 5d and Figure S12). This can be also evidenced by observing the interface resistances using the electrochemical impedance spectroscopy analyses. The NiOOH resistance increased to ~ 5.5 kΩ in the 300-ALD-cycle photoanode compared to that of ~ 1 kΩ for 200-ALD-cycle photoanode (Figure S13). Over-deposition 500-ALD-cycle NiO largely increased the NiOOH resistance to ~ 55 kΩ and significantly decreases the PEC performance.

To further discuss the enhanced PEC performances with the CoO_x and NiO modifications, the open circuit photovoltage (OCP) of the photoanodes in the same solution of 0.1 M KPi at pH 7 in dark and under AM 1.5G illumination were measured. OCP ≡ open circuit voltage upon AM 1.5G illumination (OCV_{light}) - open circuit voltage in dark (OCV_{dark}, also known as resting potential) represents the amount of the band bending at the time being with respect to that in the dark condition, for each of the constructed electrode structures. OCV is the most positive in dark due to the largest energy band upward bending, and OCV is more cathodic under illumination, with the energy band rather flattened by photoexcited carriers³⁹⁻⁴¹. The degree of the band bending is determined by the built-in potential in the photoanode/electrolyte

1
2
3
4
5
6
7
8
9
10
11
12
13
14
15
16
17
18
19
20
21
22
23
24
25
26
27
28
29
30
31
32
33
34
35
36
37
38
39
40
41
42
43
44
45
46
47
48
49
50
51
52
53
54
55
56
57
58
59
60

junction, the minority carrier accumulation and the charge recombination. An enlarged band bending at the photoanode/electrolyte interface represents the enhanced electron-hole separation. We demonstrate that the conformal deposition of *p*-type NiO on the CoO_x/BiVO₄ surface effectively enlarges the band bending. The OCP is systematically increased from the bare BiVO₄ to the CoO_x/BiVO₄ and to the 200-ALD-cycle NiO/CoO_x/BiVO₄ photoanode (Figure 5c). OCP decreases in the 300-ALD-cycle NiO/CoO_x/BiVO₄ photoanode, presumably because of the increased electron-hole recombination in the thick NiOOH film. The OCPs is repeatable under intermittent irradiation (Figure 5c) and consistent with the corresponding PEC performances. Note that kinetic or catalytic effect should be ruled out in the open circuit condition as current arising from the assumed redox reactions does not pass steadily. These observations indicate that the formation of an enlarged band bending at the photoanode/electrolyte junction is decisive for the high PEC performance⁸.

The schematic illustrations of the band bending corresponding to the measured absolute OCV_{dark} and OCV_{light} values of the bare BiVO₄, the CoO_x/BiVO₄ and the NiO/CoO_x/BiVO₄ photoanodes are shown in Figure S14. The more cathodic OCV_{light} values indicate the flattened energy band of the photoanodes (in light quasi-equilibrium with the electrolyte) by the photoexcited carriers. OCV_{light} is mostly determined by the negatively Fermi level shifts in the photoanode materials under illumination. In contrast, the OCV_{dark} reflects the upward band bending nature of the photoanodes in dark equilibrium with the electrolyte. More positive OCV_{dark} values were obtained with the NiO/CoO_x/BiVO₄ samples suggesting the effective passivation of the BiVO₄ surface states for the reduced surface Fermi leveling pinning effect. As a result, the enlarged band bending was formed after the conformal ALD NiO deposition. It is necessary to mention that our OCV measurements were performed under Ar bubbling conditions, which is the same condition in the PEC photocurrent measurements. In addition, the Ar bubbling rules out the possibility of the surface states passivation by the surface O₂ absorption in the O₂ saturated electrolyte. Therefore, we can conclude that the improved OCPs were realized at the photoanode/electrolyte junction by the conformal ALD NiO surface modifications.

Another way to probe the photoanode/electrolyte junction quality is to study the lifetime of the mobile photogenerated carriers as a function of OCP. At the transient from the illuminated quasi-equilibrium of the most flattened energy band to the dark equilibrium of the most bent energy band at the OC condition, the charge recombination is mainly determined by the spatial charges built in the photoanode/liquid junction. The enlarged band bending enables the increased amount of spatial charges in the depletion region and thus the charge recombination is enhanced at the transient when the illumination is

stopped³⁹. As a result, a fast OCP-decay is expected (Figure 5c). Using the equation developed by Zaban and Bisquert *et al.*³⁹,

$$\tau = -\frac{k_B T}{e} \left(\frac{dOCP}{dt} \right)^{-1},$$

where τ is the carrier lifetime, $k_B T$ is the thermal energy, and e is the positive element charge, the carrier lifetime can be quantified for comparison of the charge recombination rate in the junction.

In the NiO/CoO_x/BiVO₄ photoanodes, the carrier lifetime is ~ 40 ms at the transient when the illumination is stopped at the open-circuit condition in 0.1 M KPi buffer solution at pH 7 (Figure 5b). It is decreased by a factor of 25 compared to that of ~ 1 s for the CoO_x/BiVO₄ photoanode. This is indicative of the enhanced charge recombination when illumination is stopped. Consequently, the enhanced charge separation is expected in the same junction under illumination. Note that the fast OCP-decay behavior for the NiO/CoO_x/BiVO₄ photoanodes is obtained in the pH 7 electrolyte in which the OH⁻ concentration is relatively small compared to that in the high pH electrolyte. It suggests the *in-situ* formed hydroxyl-rich NiOOH on the NiO/CoO_x/BiVO₄ surface improves the BiVO₄/CoO_x/NiO/NiOOH/electrolyte solid/liquid junction quality.

Note that the conformal *p*-type NiO surface passivation could prevent the surface trapped electrons to be in direct contact with the electrolyte and therefore reduce the surface charge recombination. To further study that the surface passivation effect for BiVO₄, we deposited 5 and 10 nm conformal ALD Al₂O₃ layers over the CoO_x/BiVO₄ photoanodes, because Al₂O₃ is widely used as a dielectric passivation layer for both *p*-type and *n*-type silicon to reduce the interface charge recombination in solar cell devices. It is found that the fast OCP-decay behavior is obtained with the Al₂O₃/CoO_x/BiVO₄ photoanodes, indicating that the free mobile photogenerated carriers are improved after the Al₂O₃ surface passivation⁷ (Figure S15). However, the OCP values decrease with the increased ALD cycles of Al₂O₃. This is because the dielectric Al₂O₃ does not offer *p/n* junction effect to enlarge the band bending at the photoanode surface. In addition, the OER activity of Al₂O₃ is negligible compared to that of NiO resulting in the decreased PEC performances. It is therefore suggested that the high-efficiency charge separation and the high-performance OER activity are both the rate-determine factors for PEC OER activity.

Finally, a parametric study was performed by changing the amount of CoO_x and fixing the 200-cycles ALD NiO to quantify the CoO_x and NiO amount on BiVO₄ for the best PEC performance. The SEM images of the different amount CoO_x-loaded BiVO₄ samples are shown in Figure S16. The excessive loading of CoO_x (1.5 wt%) leads to the aggregation of the CoO_x/BiVO₄ particles during the post-annealing process, resulting in the decreased PEC per-

performances. The experimental results confirm that the NiO/CoO_x/BiVO₄ with 1 wt% CoO_x realizes the best PEC performances (Figure S17).

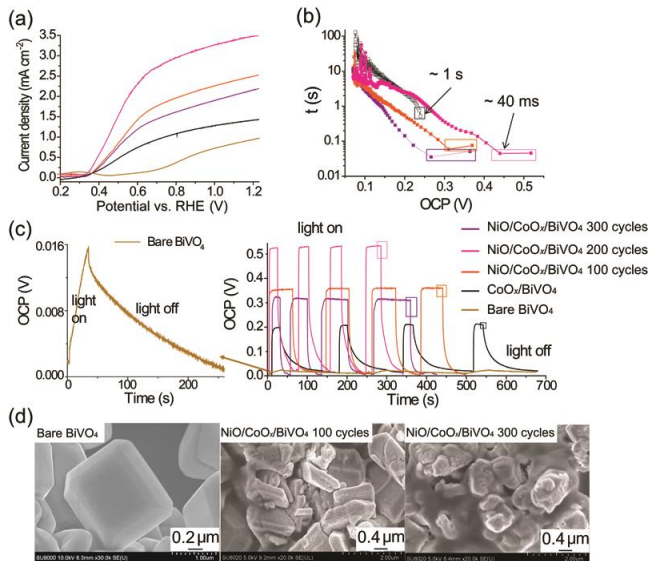


Figure 5. ALD NiO thickness dependent study. (a) The LSV scans under AM 1.5G illumination of the bare BiVO₄, the CoO_x/BiVO₄ (CoO_x 1wt%) and NiO/CoO_x/BiVO₄ (ALD 100, 200 and 300 cycles, CoO_x 1wt%) photoanodes in 0.1 M KPi solution at pH 7. (b) The carrier lifetime derived from OCP-decay curve at the transient when illumination is removed at the OC condition and plotted as a function of OCP in a logarithm scale. The results were measured in 0.1 M KPi solution at pH 7. (c) The OCP values in 0.1 M KPi solution at pH 7 under AM 1.5G illumination and in dark. (d) SEM images of the bare/BiVO₄, the 100-cycle NiO/CoO_x/BiVO₄ and 300-cycle NiO/CoO_x/BiVO₄ photoanodes after the PEC measurement.

Conclusions

In summary, we have constructed stable and efficient NiO/CoO_x/BiVO₄ photoanodes for solar water splitting. The photocurrent densities of the ~ 6 nm NiO deposited NiO/CoO_x/BiVO₄ photoanode reach 3.5 mA cm⁻² at 1.23 V_{RHE} and 2.5 mA cm⁻² at the small applied potential of 0.6 V_{RHE}, which are two-fold and three-fold increase compared to that of the CoO_x/BiVO₄ photoanode. The half-cell solar-to-hydrogen conversion efficiency is up to 1.5% and stoichiometric oxygen and hydrogen are continuously generated with Faraday efficiency of unity over 12 hours. The large PEC improvement is achieved owing to the conformal deposition of the ultrathin *p*-type NiO on the CoO_x/BiVO₄ photoanode for the effective surface states passivation and the enhanced charge separation as evidenced by the enlarged OCP value of ~ 0.53 V with a fast OCP-decay dynamics indicating the increased mobile photogenerated carriers. Further, the *in-situ* formed NiOOH on the photoanode enables a hydroxyl-rich and hydroxyl-ion permeable surface for the dual catalyst effect of CoO_x and NiOOH to improve the OER activities. The present study demonstrates that the high-efficiency

charge separation by ultrathin *p*-type surface modification can effectively improve the PEC performances. This strategy can be applied to other earth-abundant semiconductors with small band gap for wide-energy-range light absorption toward low-cost device for efficient solar fuel generation.

ASSOCIATED CONTENT

Supporting Information

The experimental details of the fabrication of the BiVO₄ photoanodes, the electrochemical characterization of the ALD NiO on FTO (Figure S1), the ALD NiO growth rate (Figure S2), the SEM images of the conformal ALD NiO on the BiVO₄ particles (Figure S3), the Mott-Schottky analyses for the ALD NiO layers (Figure S4), the chopped-light positive-bias-to-negative-bias LSV scans of the BiVO₄ and the ALD-200-cycle NiO/CoO/BiVO₄ photoanodes (Figure S5), the IPCE characterizations (Figure S6), the SEM images of the BiVO₄ and the ALD-200-cycle NiO/CoO/BiVO₄ photoanodes before and after PEC measurements (Figure S7), the decrease of the photoanodic current with the CoO_x/BiVO₄ photoanodes in LSV scans in new KPi solutions (Figure S8), dark water electrolysis with the CoO_x and NiO/CoO_x electrodes (Figure S9), the details of the NiOOH synthesis with XRD characterizations (Figure S10), the PEC performances of different BiVO₄ photoanodes in SO₃²⁻ containing solutions (Figure S11), the SEM images of the ALD-(100-300)-cycle NiO/CoO_x/BiVO₄ photoanodes after the PEC measurements (Figure S12), electro-impedance spectroscopy of the different BiVO₄ photoanodes (Figure S13), the schematic illustrations of the band bending corresponding to the measured absolute OCV_{dark} and OCV_{light} values of different BiVO₄ photoanodes (Figure S14), the OCP-decay behavior with the Al₂O₃/CoO_x/BiVO₄ photoanodes (Figure S15), the SEM images of the (0-1.5 wt%)-loaded CoO_x/BiVO₄ samples (Figure S16), and the PEC performances of the ALD-200-cycle NiO/(0-1.5 wt%)-loaded CoO_x/BiVO₄ photoanodes (Figure S17). This material is available free of charge via the Internet at <http://pubs.acs.org>.

AUTHOR INFORMATION

Corresponding Author

domen@chemsys.t.u-tokyo.ac.jp

Notes

The authors declare no competing financial interests.

ACKNOWLEDGMENT

This work was supported by the Artificial Photosynthesis Project of the Ministry of Economy, Trade and Industry (METI) of Japan, Grant-in-Aids for Specially Promoted Research (no. 23000009) and for Young Scientists (B) (no. 25810112) of the Japan Society for the Promotion of Science (JSPS). A part of work was conducted in Research Hub for Advanced Nano Characterization, The University of Tokyo, supported by the Ministry of Education, Culture, Sports, Science and Technology (MEXT), Japan. M. Z. thanks Dr. Chaoxia Yuan for the discussions.

REFERENCES

- (1) Fujishima, A.; Honda, K. *Nature* **1972**, *238*, 37-38.
- (2) Khaselev, O.; Turner, J. A. *Science* **1998**, *280*, 425-427.
- (3) Gratzel, M. *Nature* **2001**, *414*, 338-344.
- (4) Walter, M. G.; Warren, E. L.; McKone, J. R.; Boettcher, S. W.; Mi, Q.; Santori, E. A.; Lewis, N. S. *Chem. Rev.* **2010**, *110*, 6446-6473.
- (5) Reece, S. Y.; Hamel, J. A.; Sung, K.; Jarvi, T. D.; Esswein, A. J.; Pijpers, J. J. H.; Nocera, D. G. *Science* **2011**, *334*, 645-648.
- (6) Hisatomi, T.; Kubota, J.; Domen, K. *Chem. Soc. Rev.* **2014**, *43*, 7520-7535.
- (7) Formal, F. L.; Tétreault, N.; Cornuz, M.; Moehl, T.; Grätzel, M.; Sivula, K. *Chem. Sci.* **2011**, *2*, 737-743.
- (8) Du, C.; Yang, X.; Mayer, M. T.; Hoyt, H.; Xie, J.; McMahon, G.; Bischofing, G.; Wang, D. *Angew. Chem. Int. Ed.* **2013**, *52*, 12692-12695.
- (9) Kenney, M. J.; Gong, M.; Li, Y.; Wu, J. Z.; Feng, J.; Lanza, M.; Dai, H. *Science* **2013**, *342*, 836-840.
- (10) Li, Y. B.; Zhang, L.; Torres-Pardo, A.; González-Calbet, J. M.; Ma, Y.; Oleynikov, P.; Terasaki, O.; Asahina, S.; Shima, M.; Cha, D.; Zhao, L.; Takanabe, K.; Kubota, J.; Domen, K.; *Nat. Commun.* **2013**, *4*, 2566-1-2566-7.
- (11) Minegishi, T.; Nishimura N.; Kubota, J.; Domen, K.; *Chem. Sci.* **2013**, *4*, 1120-1124.
- (12) Kibria, M. G.; Zhao, S.; Chowdhury, F. A.; Wang, Q.; Nguyen, H. P. T.; Trudeau, M. L.; Guo, H.; Mi, Z.; *Nat. Commun.* **2014**, *5*, 3825-1-3825-6.
- (13) Hu, S.; Shaner, M. R.; Beardslee, J. A.; Lichterman, M.; Brunschwig, B. S.; Lewis, N. S.; *Science* **2014**, *344*, 1005-1009.
- (14) Boettcher, S. W.; Warren, E. L.; Putnam, M. C.; Santori, E. A.; Turner-Evans, D.; Kelzenberg, M. D.; Walter, M. G.; McKone, J. R.; Brunschwig, B. S.; Atwater, H. A.; Lewis, N. S.; *J. Am. Chem. Soc.* **2011**, *133*, 1216-1219.
- (15) Adriana Paracchino, A.; Laporte, V.; Sivula, K.; Grätzel, M.; Thimsen, E.; *Nat. Mater.* **2011**, *10*, 456-461.
- (16) Lee, M. H. Takei, K.; Zhang, J.; Kapadia, R.; Zheng, M.; Chen, Y.; Nah, J.; Matthews, T. S.; Chueh, Y.; Ager, J. W.; Javey, A.; *Angew. Chem. Int. Ed.* **2012**, *51*, 10760-10764.
- (17) Jacobsson, T. J.; Fjällström, V.; Sahlberg, M.; Edoffb, M.; Edvinsson, T.; *Energy Environ. Sci.* **2013**, *6*, 3676-3683.
- (18) Moriya, M.; Migeishi, T.; Kumagai, H.; Katayama, M.; Kubota, J.; Domen, K. *J. Am. Chem. Soc.* **2013**, *135*, 3733-3735.
- (19) Rao, P. M.; Cai, L.; Liu, C.; Cho, I. S.; Lee, C. H.; Weisse, J. M.; Yang, P.; Zheng, X.; *Nano Lett.* **2014**, *14*, 1099-1105.
- (20) Schuhl, Y.; Baussart, H.; Delobel, R.; Bras M. L.; Leroy, J.-M.; Gengembre, L.; Grimblot, J.; *J. Chem. Soc., Faraday Trans. 1* **1983**, *79*, 2055-2069.
- (21) Zhang, F.; Yamakata, A.; Maeda, K.; Moriya, Y.; Takata, T.; Kubota, J.; Teshima, K.; Oishi, S.; Domen, K. *J. Am. Chem. Soc.* **2012**, *134*, 8348-8351.
- (22) Tilley, S. D.; Cornuz, M.; Sivula, K.; Grätzel, M. *Angew. Chem. Int. Ed.* **2010**, *49*, 6405-6408.
- (23) Shi, X.; Choi, I. Y.; Zhang, K.; Kwon, J.; Kim, D. Y.; Lee, J. K.; Oh, S. H.; Kim, J. K.; Park, J. H.; *Nat. Commun.* **2014**, *5*, 4775-1-4775-8.
- (24) Kim, T. W.; Choi, K.-S. *Science* **2014**, *343*, 990-994.
- (25) Abdi, F. F.; Han, L.; Smets, A. H. M.; Zeman, M.; Dam, B.; Krol, R. V. D. *Nat. Commun.* **2013**, *4*, 2195-1-2195-7.
- (26) Zhong, M.; Ma, Y.; Oleynikov, P.; Domen, K.; Delaunay, J.-J. *Energy Environ. Sci.* **2014**, *7*, 1693-1699.
- (27) Thimsen, E.; Martinson, A. B. F.; Elam, J. W.; Pellin, M. J.; *J. Phys. Chem. C* **2012**, *116*, 16830-16840.
- (28) Greiner, M. T.; Helander, M. G.; Tang, W.; Wang, Z.; Qiu, J.; Lu, Z.; *Nat. Mater.* **2012**, *11*, 76-81.
- (29) Zhao, Y.; Jermamdez-Pagan, E. A.; Vargas-Barnosa, N. M.; Dysart, J. L.; Mallouk, T. E.; *J. Phys. Chem. Lett.* **2011**, *2*, 402-406.
- (30) Zhong, D. K.; Cornuz, M.; Sivula, K.; Grätzel, M.; Gamelin, D. R.; *Energy Environ. Sci.* **2011**, *4*, 1759-1764.
- (31) Dong, Y.; He, K.; Yin, L.; Zhang, A.; *Nanotechnology* **2007**, *18*, 435602-1-435602-6.
- (32) Trotochaud, L.; Young, S. L.; Ranney, J. K.; Boettcher, S. W.; *J. Am. Chem. Soc.* **2014**, *136*, 6744-6753.
- (33) Lin, F.; Boettcher, S. W. *Nat. Mater.* **2013**, *13*, 81-86.
- (34) Gardner, G. P.; Go, Y. B.; Robinson, D. M.; Smith, R. F.; Hadermann, J.; Abakumov, A.; Greenblatt, M.; Dismukes, C.; *Angew. Chem. Int. Ed.* **2012**, *51*, 1616-1619.
- (35) Kanan, M. W.; Nocera, D. G. *Science* **2008**, *321*, 1072-1075.
- (36) Barroso, M.; Cowan, A. J.; Pendlebury, S. R.; Grätzel, M.; Klug, D.; Durrant, J. R.; *J. Am. Chem. Soc.* **2011**, *133*, 14868-14871.
- (37) Lindahl, E.; Ottosson, M.; Carlsson, J.-O.; *Chem. Vap. Deposition* **2009**, *15*, 186-191.
- (38) Miikkulainen, V.; Leskelä, M.; Ritala, M.; Puurunen, R. L.; *J. Appl. Phys.* **2013**, *113*, 021301-95.
- (39) Zaban, A.; Greenshtein, M.; Bisquert, J. *Chem. Phys. Chem.* **2003**, *4*, 859-864.
- (40) Schlichtoirl, G.; Huang, S. Y.; Sprague J.; Frank A. J. *J. Phys. Chem. B*, **1997**, *101*, 8141-8155.
- (41) Fisher, A. C.; Peter, L. M.; Ponomarev, E. A.; Walker, A. B.; Wijayantha, K. G. U. *J. Phys. Chem. B* **2000**, *104*, 949-958.

TOC

